Mechanical characterization by mesoscale indentation: Advantages & pitfalls for tissue and scaffolds

Andrés Rubiano[1], Carly Galitz[2], and Chelsey S. Simmons[1,3,4]*

[1]Department of Mechanical and Aerospace Engineering, Herbert Wertheim College of Engineering; [2]Department of Mathematics, College of Liberal Arts and Sciences; [3]J. Crayton Pruitt Family Department of Biomedical Engineering Herbert Wertheim College of Engineering; [4]Division of Cardiovascular Medicine, College of Medicine, University of Florida, Gainesville, FL.

Andrés Rubiano, P.O. Box 116250, Gainesville, FL 32611
Telephone: (202) 297-8426, Fax: (352) 392-7303, Email: ssjandres@ufl.edu

Carly Galitz, P.O. Box 116250**,** Gainesville, FL 32611
Telephone: (305) 972-6928, Fax: (352) 392-7303, Email: cgalitz09@ufl.edu

***Corresponding Author:**
Chelsey S. Simmons, P.O. Box 116250, Gainesville, FL 32611
Telephone: (352) 392-4365, Fax: (352) 392-7303, Email: css@ufl.edu

ABSTRACT

Regenerative medicine and tissue engineering are hindered by the lack of consistent measurements and standards for the mechanical characterization of tissue and scaffolds. Indentation methods for soft matter are favored because of their compatibility with small, arbitrarily shaped samples, but contact mechanics models required to interpret data are often inappropriate for soft, viscous materials. Here, we demonstrate indentation experiments on a variety of human biopsies, animal tissue, and engineered scaffolds, and we explore the complexities of fitting analytical models to these data. Although objections exist to using Hertz contact models for soft, viscoelastic biological materials since soft matter violates their original assumptions, we demonstrate the experimental conditions that enable consistency and comparability (regardless of arguable misappropriation). Appropriate experimental conditions involving sample hydration, the indentation depth, and the ratio of the probe size to sample thickness enable repeatable metrics that are valuable when comparing synthetic scaffolds and host tissue, and bounds on these parameters are carefully described and discussed. We have also identified a reliable quasi-static parameter that can be derived from indentation data to help researchers compare results across materials and experiments. Although Hertz contact mechanics and linear viscoelastic models may constitute oversimplification for biological materials, the reporting of such simple metrics alongside more complex models is expected to support researchers in tissue engineering and regenerative medicine by providing consistency across efforts to characterize soft matter.

Keywords: Tissue Mechanics, Soft Matter, Nanoindentation, Hydrogels, Scaffolds, Contact Models

Impact Statement:

To engineer replacement tissue requires a deep understanding of its biomechanical properties. Mesoscale indentation (between micron and millimeter length scales) is well-suited to characterize tissue and engineered replacements as it accommodates small, oddly shaped samples. However, it is easy to run afoul of the assumptions for common contact models when working with biological materials. Here, we describe experimental procedures and modeling approaches that allow researchers to take advantage of indentation for biomechanical characterization while minimizing its weaknesses.

1. INTRODUCTION

Biological soft tissue is a challenging material to model: it is hyperelastic, heterogeneous, and anisotropic; it consists of numerous interfaces and hierarchical structures; and it is composed of networked polymer chains and charged fluid that impart time and strain rate dependence to its mechanical properties. While sophisticated constitutive models of these tissue properties are critical for accurate mechanical behavior modeling, simple quantitative values of basic mechanical properties remain important for mechanobiology and tissue engineering research. Researchers designing their own biomaterials and scaffolds recognize the need to quantify mechanical properties carefully (1), but soft matter characterization is complex. To be useful across wide-ranging experiments, labs, and companies, simple and easy-to-compare metrics of tissue mechanics are needed to complement sophisticated constitutive models.

Young's elastic modulus, perhaps the simplest metric to describe traditional engineering materials (e.g. metal alloys and ceramics), mediates the linear relationship of uniaxial stress (force divided by area) to uniaxial strain (deformation normalized to original length) in materials within their elastic range for small strains (e.g., <1%). However, biological materials can exhibit complex fluid characteristics and are challenging to manipulate into shapes and sizes amenable to simple stress-strain calculations; thus, tissue is not easily described by the conventional Young's modulus. Common tensile and shear test equipment requires samples of standard shapes and sizes, which is not always possible with biological samples, and requires low-load transducers, which are not always standard components (Table 1) (2). To accommodate small samples of irregular sizes and to avoid testing issues, such as tissue clamping and tearing in tensile testing and asymmetrical geometries for compression, nanoindentation and atomic force microscopy (AFM) use nano- to micro-scale probes and precise sensors to contact a surface and measure corresponding deflections (3). These tools were initially optimized to characterize nanoscale features and properties of hard materials and have also proven useful at the protein and cell scales (4-6), but researchers interested in materials for biomedical applications are often interested in the mesoscale (100 μm – 1 cm) as they design higher-order structures for implantation and repair.

Here, we explore the applicability of indentation at this mesoscale to hydrated, soft matter samples. We and others have developed custom equipment capable of performing indentations at the mesoscale (7-14), but translating force-displacement data derived from

indentation into intrinsic mechanical properties remains a contentious process. As many have argued, Hertz contact models originally developed to derive an elastic modulus from indentation data on hard, elastic materials are inadequate to quantify intrinsic mechanical properties for soft matter (15,16). When applied haphazardly to soft matter, Hertz contact mechanics yields notably variable results, as we demonstrate here. However, certain conditions yield reliable and consistent effective elastic moduli from mesoscale indentation of soft matter, even using a Hertz model. This approach is not appropriate for researchers working on modeling of mechanical behavior, but the effective mechanical properties resulting from the simple models described here can inform the design of new materials by providing simple, reasonable target metrics. We report an example mechanical property derived from a modified Hertz model—the steady-state modulus (SSM), a strain-rate-independent metric also referred to in mechanics as the equilibrium modulus, aggregate modulus, infinity modulus, or permanent modulus (17)—for a variety of human tissues, animal tissues, and biomaterials as a step toward simple comparisons of tissues and scaffolds.

2. MATERIALS AND METHODS

2.1. Indentation Apparatus

Our cantilever-based system comprises a capacitive sensor to quantify deflections of the tip of a custom titanium cantilever (Figure 1) (12-14). The cantilever-based probe is displaced vertically into the sample using a software-controlled, position-encoded piezoelectric stage (P-628.1CD, Physik Instrumente). The spherical indentation probe is brought into contact with the tissue sample following a time-dependent displacement profile set by the user in custom LabVIEW code. The reacting normal force of the tissue bends the titanium cantilever, and the relative displacement of the cantilever tip is measured by a capacitive sensor (C8S-3.2-2.0 and compact driver CD1-CD6, Lion Precision) through a data acquisition card system (NI 9220 and cDAQ-9171, National Instruments). The stiffness of the cantilever (79.8 N/m), calibrated using small weights that cover the full range of the capacitive sensor, is used by the LabVIEW code to determine the normal load throughout the indentation cycle. The indentation depth is held for a certain amount of time, termed the relaxation time. This “spring-loaded” relaxation does not constitute a pure stress relaxation experiment because the probe tip is allowed to move, but the

deflection during relaxation is <5% of the typical indentation depth. Actual indentation depth is used in calculations, though, so this assumption does not affect contact model calculations. After relaxation is completed, the probe returns to its initial position (these retraction data are not included in the present analysis).

In this work, pancreas samples were indented using a hemispherical-tipped 1 mm borosilicate glass probe; all other samples were indented using a 4 mm polished ruby hemisphere or as indicated in the text. We chose to work with (hemi)spherical probes that are easily ordered with "optically smooth" finishes in a range of diameters to leverage the substantial body of literature around nanoindentation and AFM, which typically use Hertz contact models for spherical tips and flat semi-infinite substrates. While many contact models are also available for "flat punch" tips, and indeed flat tips have been used elsewhere for milli-scale indentation (9), machining and polishing a flat tip to a minimally adhesive mirror finish is beyond the capacity of most academic machine shops.

2.2. Preparation and Maintenance of Hydrogel and Tissue Samples

A wide range of synthetic, bio-derived, and tissue samples have been utilized for demonstration of mesoscale indentation. Characterization of similar materials by indentation is tabulated for reference in Supplemental Table 1 (11-13,19-28).

2.2.1. Resected Tissue Samples. Human samples of pancreas were generously provided by General Surgery at the University of Florida. Patient consent, data de-identification, and tissue procurement followed protocols approved by UF's Institutional Review Board. Twenty-five pancreas resections were analyzed: 5 normal (no histologic evidence of pancreatitis or cancer), 9 pancreatitis, and 11 pancreatic ductal adenocarcinoma tumors (13). Excised tissues were placed in DMEM-F12 media and stored on ice to maintain hydration and help preserve cell and tissue conditions during transport. The size of the sample varied substantially, but volumes generally ranged between 0.1 and 1 cm^3 with side lengths between 2-10 mm Between 7 and 13 indentations were performed depending on the size of the sample. If the smallest dimension was >4 mm, the sample was sliced in a matrix slicer (Zivic Instruments) to obtain a 3 mm thick sample with a flat indentation surface.

Murine hearts were generously provided by the Division of Cardiovascular Medicine at UF and were obtained consistent with AVMA guidelines (12). One excised Wistar-Kyoto heart was cut using a stainless-steel rat heart slicer matrix (Zivic Instruments) to obtain a 3 mm thick horizontal (transverse) ventricular slice to generate data for Figure 6C. For all tissue samples, the tissue resections, submerged in culture media, were allowed to reach ambient temperature before indentation, and indentations were carried out no more than 2 hours after resection.

2.2.2. Hydrogels. A polyacrylamide (PA) gel was polymerized from acrylamide-bisacrylamide precursor solution with ammonium persulfate and tetramethylethylenediamine initiators to generate data in Figure 4. Gel volume of 380 μL was covered with 22 mm diameter cover glass during polymerization, which resulted in ~1 mm thick disc of gel, similar to a configuration reported previously(29).

Agarose powder (UltraPure™ Agarose, Life Technologies Corporation) was diluted in water to wt% indicated, heated to approximately 70°C, and stirred for 15 minutes until the solution became transparent. The solution was transferred to petri dishes and allowed to cool to obtain ~3 mm thick agarose hydrogels. After 30 minutes of cooling at room temperature, deionized (DI) water was added to the petri dish to fully submerge the sample and maintain hydration.

Polydimethylsiloxane (PDMS) samples were produced using the CY52276 Kit (Dow Corning). The silicone samples were fabricated following manufacturer instructions by mixing a 10:1 (w:w) ratio of base to curing agent. The precursor solution was then thoroughly mixed, poured into the bottom of a 40 mm diameter petri dish, vacuum degassed for an hour, and stored in a 50°C oven overnight. A dilute Triton-X 100 1:100 solution was used to reduce adhesiveness and keep the samples submerged during indentation.

All samples were stored in fluid as indicated and indented 24-48 hours after fabrication to allow swelling to reach steady state and therefore avoid disruption of data acquisition during indentation.

2.2.3. Tissue Engineering Scaffolds. High-concentration rat tail collagen type I (Corning) was diluted with 0.02% acetic acid and combined in a 3:1 ratio with Dulbecco's Modified Eagle's Medium 5X (SIGMA Life Science) and 1 M HEPES buffer solution (Gibco by Life

Technologies) to fabricate 2 mg/mL collagen hydrogels. The precursor solution was prepared at ~4°C and then incubated at 37°C for 30 minutes to allow thermogelling. The gels were then hydrated with PBS and kept at 37°C until before indentation (between 2 and 24 hours). Decellularized bovine kidney was kindly supplied by Dr. Bradley Willenberg from the University of Central Florida and obtained through previously published methods (30). Samples were maintained in saline solution for shipping on ice, stored in saline at 4°C, and indented in PBS less than a week after receiving shipment. One 1 mm-thick slice was used to generate data in Figure 7.

2.3. Contact Mechanics Model and Modified Hertz "Transient" Modulus

Many groups use indentation to characterize soft biological materials because indentation offers advantages in the context of milli-scale, irregularly shaped samples. However, indentation methods for soft matter have been widely criticized because contact models used to convert force-displacement data to effective moduli such as the Hertz modulus were originally developed for elastic, homogenous materials and not viscoelastic, hydrated biomaterials. Conventionally, the Hertz model for a spherical indenter on an elastic half-space is as follows:

$$F(\delta) = \frac{4E_{Indentation}\sqrt{R}}{3(1-\nu^2)} \cdot \delta^{3/2} \quad [1]$$

where F is the normal force, $E_{Indentation}$ is the material's effective modulus or the elastic modulus as defined by Hertz, R is the radius of the indentation probe, ν is Poisson's ratio for the sample (see discussion in Section 2.5), and δ is the depth of probe indentation into the semi-infinite solid.

This model assumes that the indented material is linear elastic, as indicated by the use of the constant elastic modulus in the equation. However, for biological materials, the work performed by the indentation tip into the sample is only partially stored as strain energy; some energy is dissipated by viscous mechanisms. This constraint and others of the Hertz model are thoroughly discussed in **Results and Discussion**. To capture this time-dependent, energy-dissipating effect, we rewrite the traditional Hertz equation as an effective modulus that is a function of force and displacement:

$$E(F,\delta) = \frac{3F(1-\nu^2)}{4\sqrt{R}\cdot\delta^{3/2}} \quad [2]$$

where the variables are defined as in Eqn. 1. Since we have both force and displacement as a function of time from our indentation data (Figure 1), we can write the transient modulus as a function of time:

$$E_{transient}(t) = \frac{3F(t) \cdot (1 - \nu^2)}{4\sqrt{R} \cdot \delta(t)^{3/2}} \quad [3]$$

where $F(t)$ and $\delta(t)$ are the experimentally measured force and indentation depth, respectively. Time-dependent stress, force, or modulus can then be fit to visco- and/or poroelastic material models (10,26,31-33). Experimental validation of the Hertz-derived transient modulus is demonstrated and discussed below.

Estimation of error associated with Equation 3 can be determined by propagation of uncertainty (34) using typical values for force, Poisson's ratio, and displacement (Supplemental Table 2). Large error is associated with low maximum forces (<100 μN), which can be reduce by using a larger diameter probe tip if the sample area is large enough to accommodate it. With low maximum forces, propagation analysis suggests percentage error values can reach ~25%, which may or may not be sufficient to distinguish between experimental groups (e.g. healthy vs. diseased tissue).

2.4. Assignment of Poisson's Ratio

Poisson's ratio (the negative ratio of strain in one direction to that in an orthogonal direction) is straightforward to define for rigid, elastic materials; however, the concept is more complex for soft matter. It is commonly assumed that ν = 0.5 for "incompressible" biomaterials, but values for biological materials may be lower because long polymer chains and fluid flow allow some volume loss that can be interpreted as compressibility. Experimental determination of Poisson's ratio is challenging because test coupons of tissue have different properties than intact tissue and because the boundary conditions of the test configuration substantially change the results. Thus, uncertainty is present with any assumed Poisson's ratio used in Equations 1-3. For simplicity, we used ν = 0.5 for all calculations; a propagation of uncertainty calculation for Equation 3 reveals that a variation of ν between 0.3 and 0.5 results in a deviation ~10%. For compliant samples, this variability is equivalent to or less than error from other sources (Supplemental Table 2), but for stiff samples, the estimate for Poisson's Ratio may be the main

source of variability and should be validated carefully if differences between experimental groups are also ≤10%.

2.5. Submersion Conditions

To submerge resected tissue, samples are placed in contact with a dry polystyrene surface before adding saline or culture medium to leverage adhesive properties of tissue. To reduce fluid volume and buoyancy forces that may detach tissue, we typically fabricate custom sample chambers by filling petri dishes with silicone (e.g. Sylgard 184, Dow Corning), storing cured dishes covered at room temperature, and punching out a chamber with a diameter 10-20% larger than the tissue sample (Figure 1A inset). In some cases, adhesion and sample weight are not enough to counteract buoyancy, in which case a small drop of surgical glue can be applied to the outer edge of the dry chamber before placing sample. Care should be taken with this approach to use large surface area samples (>1.5 cm side length) and small amounts of glue as we have found these acrylate-based glues to rapidly diffuse into the tissue and cause dramatic stiffening. We did not use this technique for any other samples reported in this manuscript, though.

Engineered samples, prepared for indentation *in situ*, typically adhere to chamber after polymerization sufficiently to avoid flotation. For our demonstration of surface adhesion, three materials over a relatively wide range of SSM values were selected as case studies: 2 mg/mL collagen hydrogels (~500 Pa), 4.5% acrylamide/0.075% bisacrylamide hydrogels (~2 kPa), and CY52276 silicone (~30 kPa). Samples were indented “dry” first, which for collagen and PA hydrogels meant that the surface layer of fluid was allowed to evaporate for 10-15 mins before indentation. The indentation probe was manually positioned close to—but not in contact with—the surface of the samples before the computer-controlled indentation cycle was initiated. After each sample was indented, it was allowed to recover for >5 mins. PBS (collagen and PA) or 5% sodium dodecyl sulfate in water (silicone) was added to fully submerge the sample and indentation tip without adjusting the indentation tip location. The sample was then re-indented under submerged conditions.

3. RESULTS AND DISCUSSION

3.1. Force-Displacement Data Do Not Fit the Hertz Equation for Large Indentation Depths

In addition to constraints associated with the material and friction/adhesion mechanisms, the Hertz model is limited to very small contact areas and indentation depths. Specifically, the indenter radius should be much greater than the indentation depth, and the indentation depth should be much less than (i.e., less than ~10% of) the sample thickness; see Selby *et al*. (35) for exemplar paper with detailed discussion and experimental demonstration of these considerations). For very compliant materials, however, suitable indentation could require a substantial contact area and/or depth to obtain measurements above the noise floor of the equipment. Large-indentation-depth violations of Hertz assumptions further render the Hertz model unsuitable for soft biomaterials (36). If materials are indented to an excessive degree (>10% thickness), Eqn. 1 cannot be fit to the data (Figure 2B) as is generally agreed upon by the nanoindentation community (37). However, when the depth of indentation remains small (≤10%), the data reasonably fit Eqn. 1 (Figure 2A, Normalized Mean Square Error (NMSE) = 0.9959) as seen in other studies (38,39). Regressions in the form of $F(\delta) = C \cdot \delta^b$ for force-displacement curves during the loading phase of indentations experiments, where both C and b are free coefficients, show that $b = 1.5$ for indentations of 10% or less of the sample thickness (Figure 2C). For our studies, the sample thickness is measured before testing using the piezoelectric stage and capacitive probe of our indentation system to confirm indentation depths less than 10% of the thickness of the sample. Since experimental force-displacement data for shallow indentations follow Hertz's $F \propto \delta^{3/2}$, "excessive indentation" beyond the 10% limit may aggravate the problems with contact models for soft materials.

3.2. Mesoscale Indentations Reduce Intra-Sample Variation

Given the clear violation of many of the original Hertz assumptions by biological materials, it is notable that the equation still describes the observed force-displacement behavior for the wide variety of soft materials we have tested. One experimental element that may be contributing to the consistent fit is our use of a relatively large millimeter-scale indentation tip (4 mm diameter). Contact bodies are assumed to be homogeneous in the Hertz contact model, but tissue samples, protein-based scaffolds, and even some synthetic hydrogels are heterogeneous. Tissue is composed of cells and cell-secreted extracellular matrix (ECM), such as hyaluronic acid, collagen fibers, and proteoglycans, among other components. Mammalian cells in tissues commonly range from 10 to 100 μm in length. The interstitial spacing between cells, filled with

ECM components and fluid, can range from 3.5 nm between connected neurons and epithelial cells to 30 μm between connected mature bone cells. Microscale probes could be probing a single cell or even between cells. Nano- and micro-scale indentations exacerbate this heterogeneity, whereas millimeter-scale indentations approach homogeneous conditions (Figure 3).

Excised tissue samples from patients are frequently small fragments that offer limited surface area for indentation, so large spherical probes with diameters on the order of sample size allow only a few indentations per sample. Probe size selection must balance between a sufficiently large probe to capture mesoscale, semi-homogeneous features and a sufficiently small probe to enable multiple indentations without artifacts from nearby indentations. We recommend the largest probe size that can achieve >3 distinct indentations while remaining two indentation lengths (~one probe diameter) away from edges and previous indents. For example, for samples prepared in a 96-well plate or an excised tissue sample <1 cm^2, a 1 mm-diameter probe could yield 4-6 indentations. For larger samples (>1.5 cm side length or diameter), probes with greater diameters (e.g. 4 mm as we discuss) reduce variance while yielding >3 indentation locations for statistical analysis or even a heat map of elastic values.

The sensitivity of our device also enables micron-scale indentation depths with micron-scale contact areas, avoiding known nonlinear deformation of polymers and soft matter at large deformations. However, the material is also assumed to be isotropic in the Hertz model, which remains an important restriction. In gelatin-alginate hydrogels that polymerize in organized, oriented fibers, we detected different effective moduli in orthogonal directions, warranting a model that reflects this anisotropy (Supplementary Figure A).

3.3. Importance of Minimizing Adhesion and Finding the Sample Surface

3.3.1. *Submersion of samples sharply suppresses adhesion.* The original Hertz contact model assumes no adhesion or friction during indentation. The presence of adhesion dramatically affects analyses of the hysteresis and hysteresis loss factor (elastic strain energy ratio) for loading-unloading indentation cycles.(3) In stress relaxation experiments, which do not incorporate the unloading phase of the force-displacement profiles, high adhesion between

surfaces may still cause inaccuracies during the loading stage (40,41). However, submersion detectably decreases the adhesiveness of most samples and can eliminate adhesion for hydrogels at the mesoscale (42). Adhesive "snap-in" can be detected while approaching a relatively dry sample (Figure 4, left column). The measured forces are close to zero until adhesive forces pull the tip onto the surface, at which point the forces transition to negative values and slowly start increasing as the indentation probe continues to move into the sample. Unlike indentation on dry samples, submerged indentations show a consistent linear increase due to buoyancy, followed by the successively increasing force that characterizes Hertz contact (Figure 4, right column).

3.3.2. Accurate surface finding is required to use the transient modulus. The development of indentation systems for traditional engineering materials has generated multiple techniques for accurately finding the surface before indentation, but these techniques are confounded in soft biological materials because of low contact forces and the possibility of adhesion forces. Consensus is that most hydrogels and tissue samples are submerged to maintain hydration—avoiding sample shrinkage and cell death—and to meet the low adhesion requirement previously discussed.

It is computationally critical, however, to know exactly when the probe first makes contact with the surface (43-46), and buoyancy forces can easily be confounded with contact forces as the tip moves closer to the sample before actual contact. This increase in buoyancy is easier to detect when linear as it can be differentiated from the curved loading stage of the indentation, assuming that linearity is ensured using constant-diameter indentation shafts (Figure 5A). A simple approach to locating the sample surface is to carry out a linear regression for the group of points starting at time zero and ending in a variable time, t. The time for which this regression is no longer linear (corresponding to a low coefficient of determination) can be used to assume the position for which the probe makes contact with the sample (Figure 5).

When using the transient modulus to calculate SSM, it is imperative to identify the surface of the sample accurately. In general, the distorted curvature of force-displacement curves resulting from inaccurate surface detection can result in fitting to inappropriate contact models (47). For the models described here, initiating an indentation routine with inaccurate identification of the sample surface can result in unreliable values for effective moduli, transient moduli, and the SSM (Supplementary Figure B). If an indentation begins away from the surface (out of contact), a Hertzian regression does not fit the initial indentation data well but the SLS fit

to transient modulus is reasonable (Supplementary Figure B-A,A'); however, the SLS fit results in misleadingly low SSM values compared to appropriately indented samples (Supplementary Figure B-B,B'). If a sample is erroneously pre-indented, the Hertz fit for the loading stage and SLS fit will be reasonable, but the SLS fit will yield an artificially high SSM (Supplementary Figure B-C,C'). Consequently, our recommendation is to confirm that the transient modulus during the loading stage (before relaxation) fluctuates around a value that is similar to the Hertz-derived effective modulus of the indentation phase (Supplementary Figure B-B,B').

3.4. The Effective Modulus from the Hertz Contact Model Is Strain-Rate Dependent

The Hertz contact model assumes linear elastic, homogenous, and isotropic properties—idealizations that often do not apply to biological tissues. Furthermore, the surfaces must be frictionless, smooth, and adhesion-less to satisfy the Hertz assumptions. However, with careful experimental controls, *the form* of the Hertz contact model as in Eqn. 1 does fit well to indentations of soft biological materials (Figure 2A). Note that for soft matter, the modulus derived from this equation cannot strictly be termed the "elastic modulus" because the material exhibits known relaxation with short time scales and because this modulus quantity varies substantially with small changes in indentation rate (Figure 6). Thus, we refer to this simplified value as the "effective modulus".

This effective modulus is challenging to compare across experiments, tissue, and labs because it depends on the indentation rate (16,41,46). For soft matter, higher indentation rates result in less time for energy dissipation and thus a higher apparent stiffness (Figure 6). The magnitude of this effect varies depending on the material, further affecting comparison and interpretation. For 0.4% agarose hydrogels, a four-fold change in indentation rate can result in a two-fold change in the obtained effective modulus (Figure 6A), while a ten-fold increase in rate results in a 50% increase in the estimated effective modulus of rat left ventricle tissue (Figure 6C). These relationships between rates and moduli are not consistent across materials, making this strain-rate dependence challenging to generalize and potentially leading to erroneous comparisons: compliant materials tested at high strain rates could appear comparable to stiffer materials tested at low strain rates.

Surfaces should also be frictionless and smooth to use the Hertz model; we use a ruby hemisphere with a smooth optical finish. No adhesion is accounted for in the Hertz model; thus,

modified Hertz-JKR models are often used to understand hysteresis in soft biomaterials when adhesion is expected and of interest (48-50). However, submersion of samples in media seems to mitigate "snap-in" (Figure 4), so we proceed with the unmodified Hertz equation to derive an effective modulus rather than attempting to describe the surface properties in more detail.

3.5. The Hertz-Derived Transient Modulus Decays to the Strain-Rate-Independent SSM

For mesoscale indentation relaxation experiments, we found that the forces rapidly decayed to a steady-state value within minutes for all soft matter tested, in keeping with other applications of indentation to stress relaxation experiments (3). Inserting this steady-state force into the Hertz model (Equation 2) yields a modulus value that approximately matches the effective modulus value fit to force-displacement data (Equation 1) obtained during quasi-static indentation (Supplementary Figure C). Given this consistency, we assumed that the rearranged Hertz equation is also useful to derive a time-dependent transient modulus as in Equation 3. The transient modulus does in fact decay to a strain-rate-independent SSM for all biological materials that we have tested, including decellularized porcine kidney (Figure 7), rat myocardium (12), and human tumors (13,14). The concept of such an infinite, equilibrium, or aggregate modulus is widely applied to viscoelastic and poroelastic materials and models. The reader is directed to reviews by Chen, Yang and Lai (17) and Oyen and Cook (51) for excellent discussion of visco/poroelastic constitutive models and analysis of transient nanoindentation data, respectively. Further, the transient-modulus-derived SSM yields similar effective modulus values to that of quasi-static loading (low strain rate, Supplementary Figure C), and the initial transient modulus matches effective modulus values for instantaneous loading conditions (high strain rate, Supplementary Figure D).

Given the broad range of mechanical properties targeted by the tissue engineering community, a wide range of strain rates and constitutive models remain relevant. However, many groups utilize similar materials for different purposes, so reporting steady-state or quasi-static parameters will help the community compare data across projects, tissues, and scaffolds. Performing stress-relaxation experiments, fitting transient data to visco/poroelastic models, or performing quasi-static indentation with optical methods (19,24) will yield SSM and other quasi-static parameters that would be more comparable across methods and models. Future tissue engineering applications will dictate whether a given material's response to either low or high

strain rates is notable, e.g., low-strain-rate expansion during development versus high-strain-rate shock waves through the brain. In any case, the transient modulus approach provides these and intermediate response values from only one relaxation experiment, in stark contrast to a single indentation-retraction pass yielding one strain-rate-dependent metric that may not be comparable with other labs, materials, or experiments. However, more complex and nuanced experiments, contact models, and constitutive models are still needed to create parameters appropriate for computational models of time-dependent loading conditions.

3.6. The Stress Relaxation Modulus Can Be Fitted to Various Constitutive Models and Still Yield Similar SSM Values

Constitutive models that accurately describe time-dependent tissue behavior continue to challenge the biomaterials and biomechanics communities and require increasing levels of complexity (as discussed, for example, by Oyen and Cook (51)). To characterize the consistency of the SSM across indentation experiments and models, we used three different time-dependent constitutive models to fit the transient modulus to determine the SSM (Supplemental Table 3). While these common constitutive models vary in their estimation of the initial relaxation behavior of the materials tested, they consistently describe the semi-infinite relaxation behavior and identify similar SSM values (Supplementary Figure E). The concept of a quasi-static modulus, despite its various names, is compatible with many constitutive models and is therefore a useful value for researchers to reference when comparing experimental methods and models and producing application-specific mechanical characterization data.

4. CONCLUSIONS

Indentation methods for biological materials are contentious because most contact models have been derived for purely elastic, homogenous, and isotropic materials in an adhesion-free and frictionless experimental configuration. While many of these assumptions are violated while indenting soft matter, the general relationship derived by Hertz among force, displacement, and mechanical properties notably holds true, although the exact mechanical property defined in the equation is not the elastic modulus as originally described. The strain rate can sharply alter our measurements of what the Hertz model assumes to be a property of the material—the elastic modulus. We propose that this mechanical property should be referred to as an *effective modulus*

since it is the apparent modulus for a specific indentation rate. At very slow quasi-static indentation rates, the Hertz modulus matches the infinite modulus or SSM of the material. To use the Hertz equation for soft biological materials, millimeter-scale samples and indenter tips are recommended. Surface contact and indentation depth must be carefully controlled for the resulting values to be reliable. Furthermore, this approach is not recommended for materials that demonstrate large adhesive forces nor those known to be strongly anisotropic.

Rearrangement of the Hertz contact model equation introduces the *transient modulus* as a function of time throughout an indentation or relaxation cycle. We have demonstrated that relaxation experiments are advantageous, as they can yield multiple metrics that can be compared to other quasi-static quantities, unlike strain-rate-dependent values calculated from loading-unloading cycles. The transient modulus is a useful construct and reasonable rearrangement of the Hertz modulus as demonstrated experimentally in three ways. First, the Hertz effective modulus fit to an "instantaneous" loading is close to the same value as $E(t = 0)$ using transient modulus data fit to Equation 4 (Supplementary Figure D-A); that is, near-instantaneous loading conditions result in similar values for the effective modulus from the original Hertz equation and from the transient modulus evaluated at $t = 0$. Second, slow indentations that use loading times higher than relaxation times yield an effective modulus for quasi-steady-state conditions. This effective modulus matches values calculated for the SSM (Supplementary Figure C-A), confirming the similarity between the Hertz fit and the transient modulus. Finally, the effective modulus for any given strain rate matches the average of the transient modulus during the loading stage of the indentation (Supplementary Figure B-B). These three demonstrations suggest that time-dependent rearrangement of the Hertz equation is reasonable within the experimental constraints discussed to yield a useful transient modulus.

There is a substantial risk to promoting Hertz contact models for soft matter in that the initial indentation modulus or effective modulus may continue to be discussed as an elastic modulus, undesirably obfuscating the role of porous or viscous relaxation. However, many disciplines, and tissue engineering in particular (1), have long communicated a desire for simple, standardized ways to characterize mechanical properties of biological materials. This transient modulus and its semi-infinite SSM can be used to compare small, irregular samples of soft matter to design replacement materials and tissues in a straightforward manner. In addition, we show that the SSM can be constitutive-model independent; thus, its reporting alongside complex

constitutive models can support the diverse goals of researchers interested in mechanical properties for computational biomechanics, tissue engineering, biomaterials, and mechanobiology.

ACKNOWLEDGMENTS

The authors gratefully acknowledge partial support of this work by Medtronic (Investigator-Initiated Grant to C.S.S.), the National Science Foundation (CMMI-BMMB 1636007 to C.S.S.), and the University of Florida's Pittman Fellowship of the Institute for Cell and Tissue Science and Engineering (A.R.). We thank John M. Maloney for valuable editorial input.

AUTHOR DISCLOSURE STATEMENT

No competing financial interests exist.

REFERENCES

1. Hunsberger J, Harrysson O, Shirwaiker R, Starly B, Wysk R, Cohen P, et al. Manufacturing Road Map for Tissue Engineering and Regenerative Medicine Technologies. Stem Cells Transl Med. Wiley-Blackwell; **4**(2), 130, 2015.

2. McKee CT, Last JA, Russell P, Murphy CJ. Indentation Versus Tensile Measurements of Young's Modulus for Soft Biological Tissues. Tissue Engineering Part B: Reviews. **17**(3), 155, 2011.

3. Oyen ML. Nanoindentation of hydrated materials and tissues. Current Opinion in Solid State and Materials Science. **19**(6), 317, 2015.

4. Van Vliet K, Bao G, Suresh S. The biomechanics toolbox: experimental approaches for living cells and biomolecules. Acta Materialia. 2003.

5. Kasas S, Dietler G. Probing nanomechanical properties from biomolecules to living cells. Pflugers Arch. **456**(1), 13, 2008.

6. Holle AW, Young JL, Van Vliet KJ, Kamm RD, Discher D, Janmey P, et al. Cell–Extracellular Matrix Mechanobiology: Forceful Tools and Emerging Needs for Basic and Translational Research. Nano Lett. **18**(1), 1, 2017.

7. Cox MAJ, Driessen NJB, Boerboom RA, Bouten CVC, Baaijens FPT. Mechanical characterization of anisotropic planar biological soft tissues using finite indentation: Experimental feasibility. Journal of Biomechanics. **41**(2), 422, 2008.

8. Constantinides G, Kalcioglu ZI, McFarland M, Smith JF, Van Vliet KJ. Probing mechanical properties of fully hydrated gels and biological tissues. Journal of Biomechanics. **41**(15), 3285, 2008.

9. Levental I, Levental KR, Klein EA, Assoian R, Miller RT, Wells RG, et al. A simple indentation device for measuring micrometer-scale tissue stiffness. Journal of Physics: Condensed Matter. **22**(19), 194120, 2010.

10. Hu Y, Zhao X, Vlassak JJ, Suo Z. Using indentation to characterize the poroelasticity of gels. Applied Physics Letters. American Institute of Physics; **96**(12), 121904, 2010.

11. Sugimoto M, Takahashi S, Kojima M, Gotohda N, Kato Y, Kawano S, et al. What is the nature of pancreatic consistency? Assessment of the elastic modulus of the pancreas and comparison with tactile sensation, histology, and occurrence of postoperative pancreatic fistula after pancreaticoduodenectomy. Surgery. **156**(5), 1204, 2014.

12. Rubiano A, Qi Y, Guzzo D, Rowe K, Pepine C, Simmons C. Stem cell therapy restores viscoelastic properties of myocardium in rat model of hypertension. J Mech Behav Biomed Mater. **59**, 71, 2016.

13. Rubiano A, Delitto D, Han S, Gerber M, Galitz C, Trevino J, et al. Viscoelastic properties of human pancreatic tumors and in vitro constructs to mimic mechanical properties. Acta Biomater. **67**, 331, 2017.

14. Stewart DC, Rubiano A, Dyson K, Simmons CS. Mechanical characterization of human brain tumors from patients and comparison to potential surgical phantoms. Engler AJ, editor. PLoS ONE. Public Library of Science; **12**(6), e0177561, 2017.

15. Hertz H. Ueber die Berührung fester elastischer Körper (On the contact of rigid elastic solids). Journal für die reine und angewandte Mathematik [Internet]. **92**, 156, 1882. Available from: http://eudml.org/doc/148490

16. Nalam PC, Gosvami NN, Caporizzo MA, Composto RJ, Carpick RW. Nano-rheology of hydrogels using direct drive force modulation atomic force microscopy. Soft Matter. **11**(41), 8165, 2015.

17. Chen D-L, Yang P-F, Lai Y-S. A review of three-dimensional viscoelastic models with an application to viscoelasticity characterization using nanoindentation. Microelectronics Reliability. **52**(3), 541, 2012.

18. Gavara N. A beginner's guide to atomic force microscopy probing for cell mechanics. Toca-Herrera JL, editor. Microsc Res Tech. John Wiley & Sons, Ltd; **80**(1), 75, 2016.

19. Bashirzadeh Y, Chatterji S, Palmer D, Dumbali S, Qian S, Maruthamuthu V. Stiffness Measurement of Soft Silicone Substrates for Mechanobiology Studies Using a Widefield Fluorescence Microscope. JoVE. (137), 2018.

20. Berry MF, Engler AJ, Woo YJ, Pirolli TJ, Bish LT, Jayasankar V, et al. Mesenchymal stem cell injection after myocardial infarction improves myocardial compliance. Am J Physiol Heart Circ Physiol [Internet]. **290**(6), H2196, 2006. Available from: http://ajpheart.physiology.org/cgi/doi/10.1152/ajpheart.01017.2005

21. Engler AJ, Richert L, Wong JY, Picart C, Discher DE. Surface probe measurements of the elasticity of sectioned tissue, thin gels and polyelectrolyte multilayer films: Correlations between substrate stiffness and cell adhesion. Surface Science. **570**, 142, 2004.

22. Tse JR, Engler AJ. Preparation of Hydrogel Substrates with Tunable Mechanical Properties. Hoboken, NJ, USA: John Wiley & Sons, Inc; p. 1–16, 2001.

23. Gautreau Z, Griffin J, Peterson T, Thongpradit P. Characterizing Viscoelastic Properties of Polyacrylamide Gels [Internet]. Billiar K, Burnham N, editors. 2006. Available from: http://www.wpi.edu/Pubs/E-project/Available/E-project-042706-113033/unrestricted/Polyacrylamide_MQP_Final_Report.pdf

24. Lee SJ, Sun J, Flint JJ, Guo S, Xie HK, King MA, et al. Optically based-indentation technique for acute rat brain tissue slices and thin biomaterials. J Biomed Mater Res Part B Appl Biomater. **97**(1), 84, 2011.

25. Kenry, Leong MC, Nai MH, Cheong FC, Lim CT. Viscoelastic Effects of Silicone Gels at the Micro- and Nanoscale. Procedia IUTAM. Elsevier B.V; **12**, 20, 2015.

26. Delaine-Smith RM, Burney S, Balkwill FR, Knight MM. Experimental validation of a flat punch indentation methodology calibrated against unconfined compression tests for determination of soft tissue biomechanics. Journal of the Mechanical Behavior of Biomedical Materials. Elsevier; **60**, 401, 2016.

27. Achterberg VF, Buscemi L, Diekmann H, Smith-Clerc J, Schwengler H, Meister J-J, et al. The nano-scale mechanical properties of the extracellular matrix regulate dermal fibroblast function. J Invest Dermatol. **134**(7), 1862, 2014.

28. Lopez-Garcia MDC, Beebe DJ, Crone WC. Young's modulus of collagen at slow displacement rates. Biomed Mater Eng. IOS Press; **20**(6), 361, 2010.

29. Simmons CS, Ribeiro AJS, Pruitt BL. Formation of composite polyacrylamide and silicone substrates for independent control of stiffness and strain. Lab Chip. **13**(4), 646, 2013.

30. Willenberg BJ, Oca-Cossio J, Cai Y, Brown AR, Clapp WL, Abrahamson DR, et al. Repurposed biological scaffolds: kidney to pancreas. Organogenesis. Taylor & Francis; **11**(2), 47, 2015.

31. Rianna C, Radmacher M. Comparison of viscoelastic properties of cancer and normal thyroid cells on different stiffness substrates. Eur Biophys J. **46**(4), 309, 2016.

32. Jachowicz J, McMullen R, Prettypaul D. Indentometric analysis of in vivo skin and comparison with artificial skin models. Skin Research and Technology. Wiley/Blackwell (10.1111); **13**(3), 299, 2007.

33. Ahearne M, Yang Y, Haj El AJ, Then KY, Liu K-K. Characterizing the viscoelastic properties of thin hydrogel-based constructs for tissue engineering applications. Journal of The Royal Society Interface. **2**(5), 455, 2005.

34. Holman JP. Experimental Methods for Engineers. McGraw-Hill Higher Education; 2012.

35. Selby A, Maldonado-Codina C, Derby B. Influence of specimen thickness on the nanoindentation of hydrogels: Measuring the mechanical properties of soft contact lenses. Journal of the Mechanical Behavior of Biomedical Materials. **35**, 144, 2014.

36. Bush BG, Shapiro JM, DelRio FW, Cook RF, Oyen ML. Mechanical measurements of heterogeneity and length scale effects in PEG-based hydrogels. Soft Matter [Internet]. rsc; **11**(36), 7191, 2015. Available from: http://pubs.rsc.org/en/content/articlehtml/2015/sm/c5sm01210d

37. Fischer-Cripps AC. A review of analysis methods for sub-micron indentation testing. Vacuum. Pergamon; **58**(4), 569, 2000.

38. van Dommelen JAW, van der Sande TPJ, Hrapko M, Peters GWM. Mechanical properties of brain tissue by indentation: Interregional variation. **3**(2), 158, 2010. Available from: http://dx.doi.org/10.1016/j.jmbbm.2009.09.001

39. Finan JD, Fox PM, Morrison B. Non-ideal effects in indentation testing of soft tissues. Biomechanics and Modeling in Mechanobiology. **13**(3), 573, 2014.

40. Derjaguin BV, Muller VM, Toporov YP. Effect of contact deformations on the adhesion of particles. Journal of Colloid and Interface Science. **53**(2), 314, 1975.

41. Charitidis C. Nanoscale Deformation and Nanomechanical Properties of Soft Matter Study Cases: Polydimethylsiloxane, Cells and Tissues. ISRN Nanotechnology. Hindawi; **2011**(4), 1, 2011.

42. Megone W, Roohpour N, Gautrot JE. Impact of surface adhesion and sample heterogeneity on the multiscale mechanical characterisation of soft biomaterials. Sci Rep. Springer US; 1, 2018.

43. Dimitriadis EK, Horkay F, Maresca J, Kachar B, Chadwick RS. Determination of Elastic Moduli of Thin Layers of Soft Material Using the Atomic Force Microscope. Biophysj. Elsevier; **82**(5), 2798, 2002.

44. Kaufman JD, Klapperich CM. Surface detection errors cause overestimation of the modulus in nanoindentation on soft materials. Journal of the Mechanical Behavior of Biomedical Materials. **2**(4), 312, 2009.

45. Wei J, McFarlin BL, Wagoner Johnson AJ. A multi-indent approach to detect the surface of soft materials during nanoindentation. Journal of materials research. **31**(17), 2672, 2016.

46. Simič R, Mathis CH, Spencer ND. A two-step method for rate-dependent nano-indentation of hydrogels. Polymer. Elsevier Ltd; **137**, 276, 2018.

47. Garcia M, Schulze KD, O'Bryan CS, Bhattacharjee T, Sawyer WG, Angelini TE. Eliminating the surface location from soft matter contact mechanics measurements. Tribology - Materials, Surfaces & Interfaces [Internet]. **11**(4), 187, 2017. Available from: https://www.tandfonline.com/doi/full/10.1080/17515831.2017.1397908

48. Johnson K, Kendall K, Roberts A. Surface energy and the contact of elastic solids. Proceedings of the Royal Society of London. A. Mathematical and Physical Sciences. **324**(1558), 301, 1971.

49. Efremov YM, Bagrov DV, Kirpichnikov MP, Shaitan KV. Application of the Johnson–Kendall–Roberts model in AFM-based mechanical measurements on cells and gel. Colloids and Surfaces B: Biointerfaces. Elsevier; **134**, 131, 2015.

50. Jin C, Ebenstein DM. Nanoindentation of compliant materials using Berkovich tips and flat tips. Journal of materials research. **32**(02), 435, 2017.

51. Oyen ML, Cook RF. A practical guide for analysis of nanoindentation data. Journal of the Mechanical Behavior of Biomedical Materials. Elsevier Ltd; **2**(4), 396, 2009.

Table 1. Common mechanical characterization tools for biomaterials

	Opportunities	Challenges
Tension/ Compression Testing	Universal test equipment readily available in engineering departments, lends itself to simplest constitutive models	Load cells may not be sensitive enough, and samples hard to grip and to cut into shape with consistent cross-sectional area
Rheology	Rheometers and viscometers readily available in engineering departments, optimized for dynamic testing	May not accommodate higher modulus samples, tissue samples hard to cut into shape and test without slippage
Atomic Force Microscopy/Nano-indentation	Readily available in engineering departments, compatible with wide range of sample sizes and stiffnesses, probes with stiffnesses/diameters for soft matter available commercially (18)	Small contact diameters (<10 μm) may not reflect bulk material properties, hard to determine contact accurately
Mesoscale Indentation	Compatible with wide range of sample sizes and stiffnesses, contact diameters (~100-1000 μm) better reflect bulk properties, microscopy-based method possible (19)	Availability of commercial options limited in engineering departments compared to other techniques

Table 2. Summary of Recommendations for Indentation of Tissue and Scaffolds	
Experimental Setup and Sample Prep	• Sample is anchored to chamber • Sample surface is flat • Probe size << surface area to enable multiple indentations at least one tip diameter away from edge • Probe diameter > 250 μm for "tissue" properties rather than cell properties
Using a Hertz Contact Model	• Form of the equation matches your tip shape • Sample is submerged to minimize adhesive effects • Max indentation depth ≤10% sample thickness • Material is quasi-homogeneous at scale of contact radius, i.e., ~ ½ probe radius • Material is isotropic, i.e., no clear alignment or layers • Indentation routine begins at the surface of the sample
Reporting Your Findings	• "Modulus" and other reported metrics are clearly defined • Corresponding indentation rate(s) are clearly indicated • To facilitate comparison across labs, steady-state modulus (SSM) is reported in addition to your own parameters of interest. SSM could be derived from stress relaxation, quasi-static indentation (<1μm/s), or at equilibrium

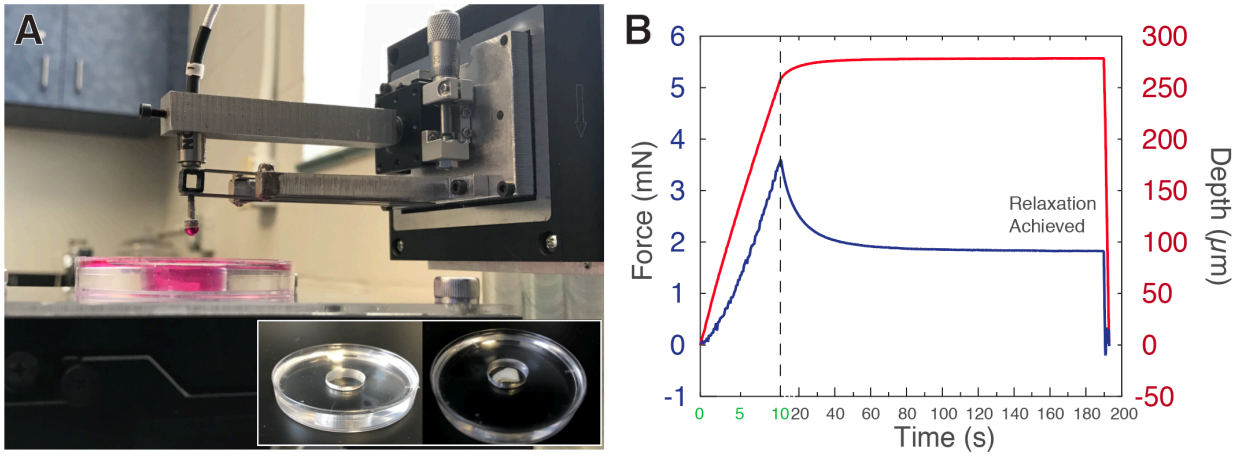

Figure 1. (A) A millimeter-scale indentation device enables mechanical characterization of biological materials. Inset depicts the silicone chamber empty (left) and with a tissue sample (right). Submerged sample shown under the indentation tip. (B) A single indentation profile for force (left axis, bottom blue line) and depth (right axis, top red line) are shown on an example hydrogel (0.6% agarose) using an open-loop displacement control system. As the displacement of the cantilever base is held constant, stress relaxation causes the calculated force to decrease over time until steady state is reached, representing the remaining elastic component of the material described by different names in various constitutive models.

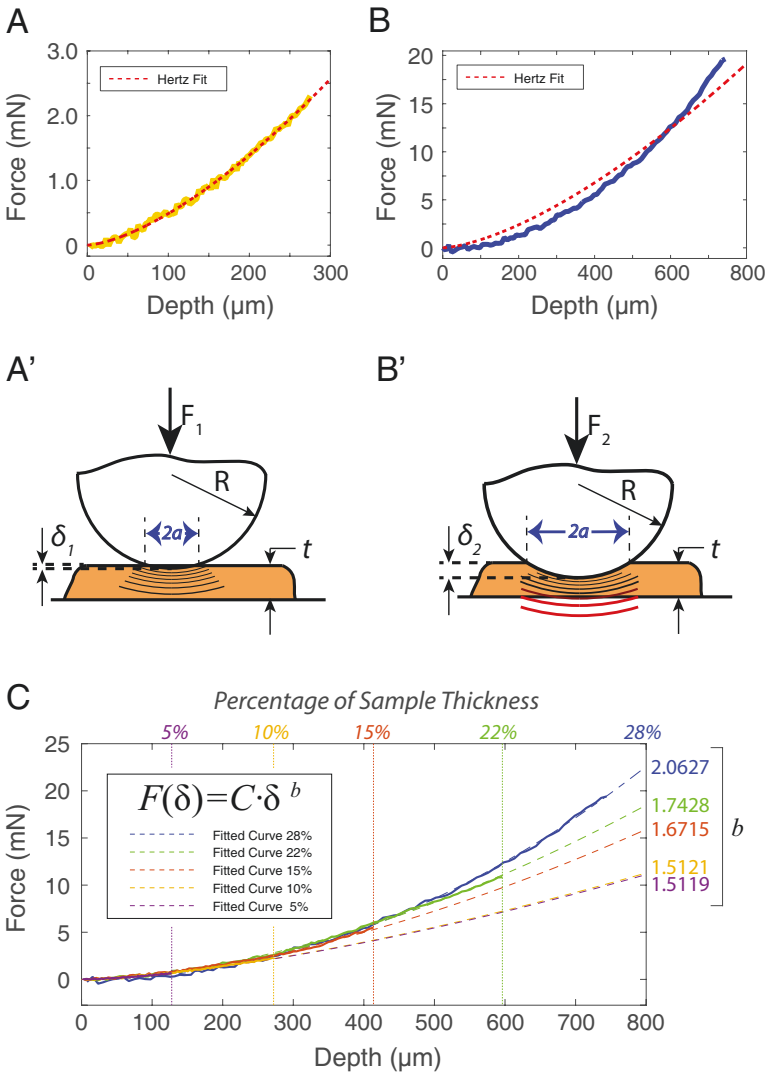

Figure 2. (A) Force-displacement data from a milli-indenter are consistent with the Hertz equation $F(\delta) = C \cdot \delta^{3/2}$ for small indentations (normalized mean square error, NMSE = 0.9959). Indentation was constrained to a 10% depth of 2.75 mm thick 0.4% agarose hydrogels at a 30 μm/s indentation rate. The radius of the indenter was 2 mm, and Poisson's ratio was assumed to be 0.4. The relative dimensions correspond more closely to schematic A'. (B) Force-displacement data do not fit the form of $F(\delta) = C \cdot \delta^{3/2}$ for >10% indentation depths (28% depth shown) on 2.75 mm thick 0.4% agarose hydrogels at a 30 μm/s indentation rate. Relative dimensions correspond more closely to schematic B'. (C) Force-displacement fits in the form of $F(\delta) = C \cdot \delta^{b}$ for various indentation depths on 2.75 mm thick 0.4% agarose hydrogels. Indentations less than or equal to 10% of the thickness of the sample display an exponential fit close to b = 3/2 as in the Hertz contact model (Equation 1), while deeper indentations show an increasing exponent with depth. All fits shown have NMSE > 0.99, where 1 is a perfect fit.

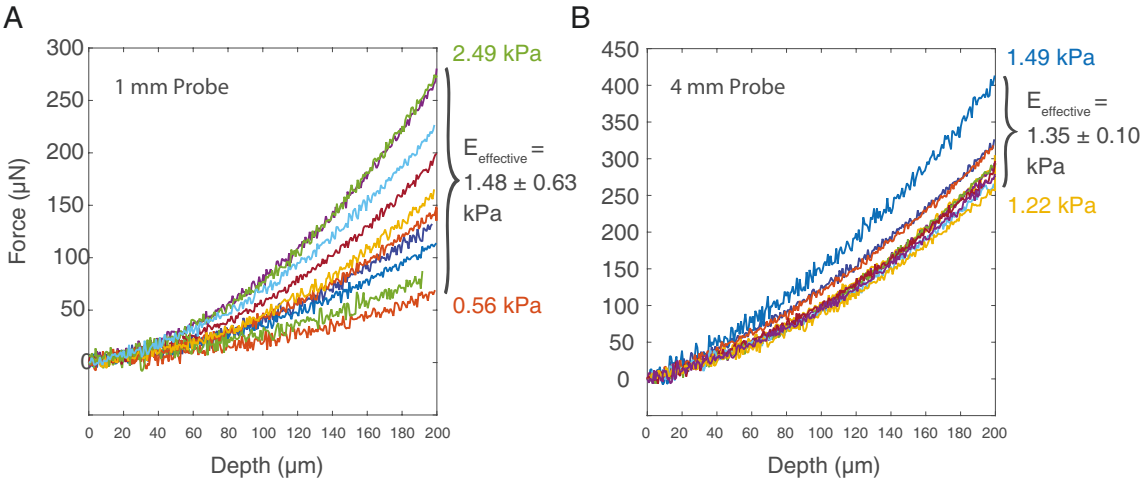

Figure 3. Hertz modulus from 10 indentations on a human pancreatitis resection using a 1 mm diameter probe (A) yields more than 6 times the standard deviation obtained from a 4 mm probe (B). Larger-diameter probes can reduce moduli variance by indenting larger areas that resemble more homogeneous structures. The probe size at which variability substantially decreases depends on the tissue complexity and scale.

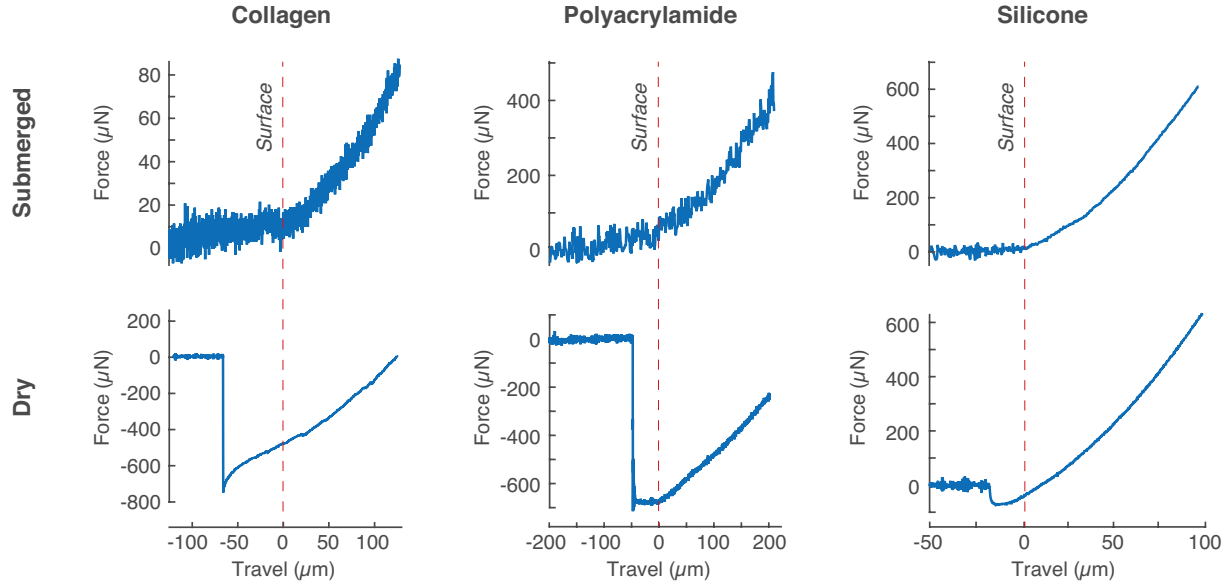

Figure 4. Force-displacement profiles for approach and loading stages show that tip-to-sample adhesion on dry samples (left column) causes Hertz fits to be inapplicable to curves immediately after contact, while submerged sample profiles (right column) show a clear transition from a linear buoyancy increase to Hertz contact behavior. Here, 2 mg/mL collagen (~500 Pa), 4.5% acrylamide/0.075% bisacrylamide PA (~2 kPa), and CY52276 silicone (~30 kPa) were used. Vertical dashed lines indicate expected contact with the sample surface absent adhesive forces. The submerged PA gel and silicone were indented at 8 μm/s and 3 μm/s, respectively. A rate of 1 μm/s was used for all other indentation experiments to reduce noise.

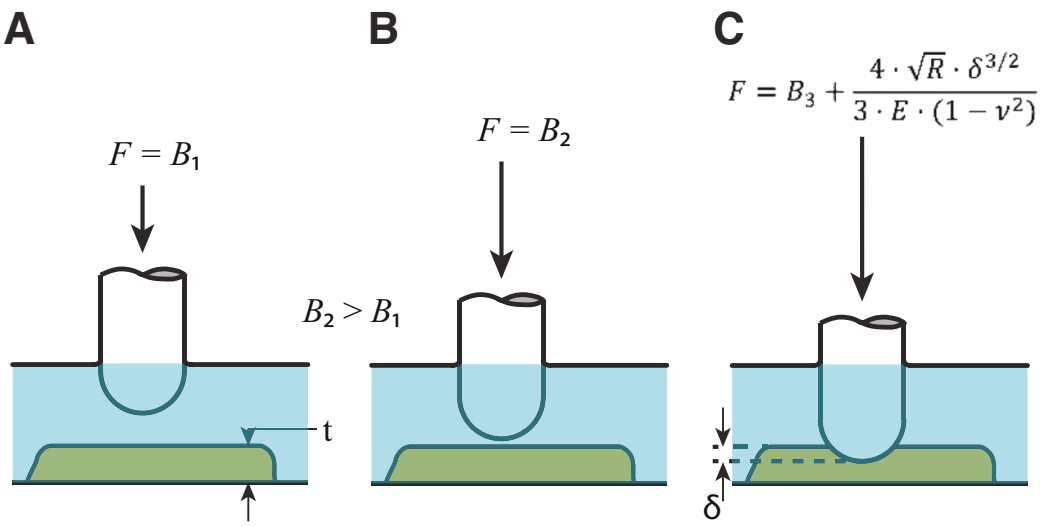

Figure 5. (A-B) The measured buoyancy force increases linearly before contact using constant-diameter shafts. (C) After contact, the measured forces include buoyancy and tip-sample interaction.

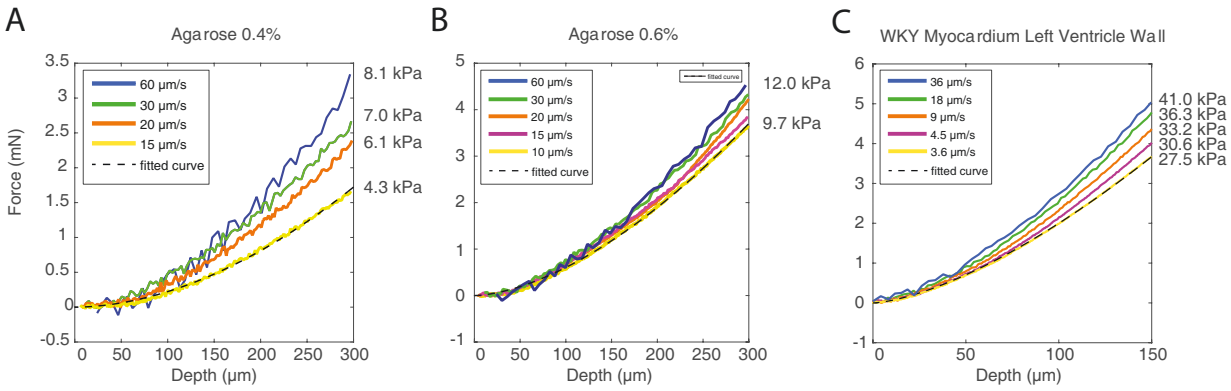

Figure 6. The indentation rate can affect the effective modulus obtained through the Hertz contact model for (A) agarose 0.4% hydrogels, (B) agarose 0.6% hydrogels, and (C) rat myocardium (WKY = Wistar-Kyoto breed). Dashed lines show the Hertz fit for the lowest strain rate, showing that even for slow indentation rates where viscous dissipation could be occurring, the form of the Hertz model $F(\delta) = C \cdot \delta^{3/2}$ remains a reasonable fit. Note the different scales for indentation depths and forces across samples.

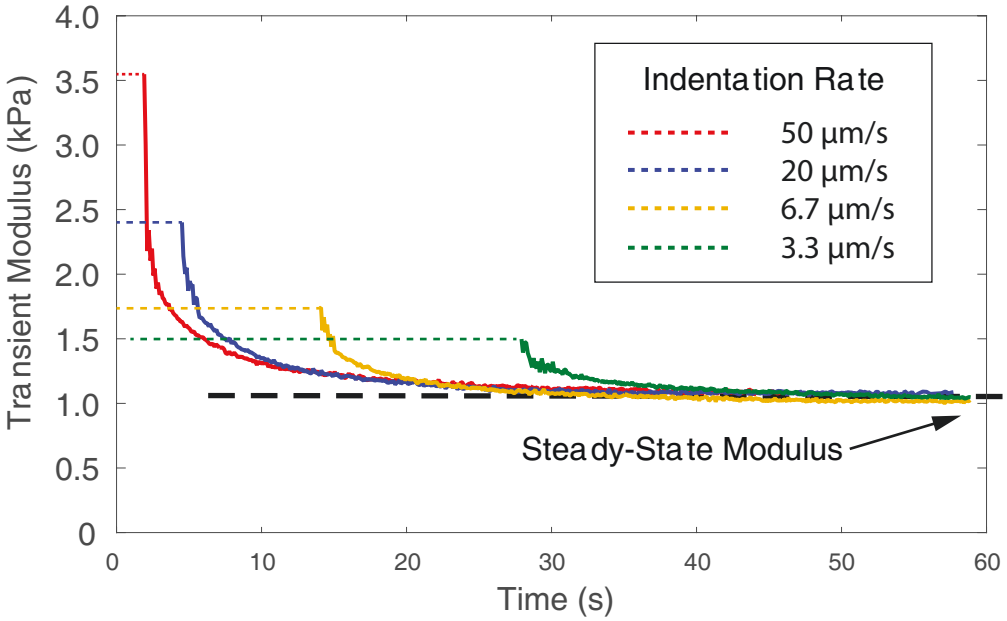

Figure 7. The SSM is consistent even for intial indentations at different displacement rates, revealing independence of the strain rate. The effective modulus that would have been calculated using the Hertz model (dashed lines) for the selected indentation rates yields values between 1.5 and 3.5 kPa. Sample: decellularized porcine kidney medulla cut to 1 mm thick slices and indented 100 µm at the designated rate.

Supplementary Material

Mechanical characterization by mesoscale indentation: Advantages & pitfalls for tissue and scaffolds

Andrés Rubiano, Carly Galitz, and Chelsey S. Simmons

Preparation and Maintenance of Hydrogel and Tissue Samples

A. Resected Tissue Samples. Human brain tumors were generously provided by the Florida Center for Brain Tumor Research. Patient consent, data de-identification, and tissue procurement were consistent with protocols approved by UF's Institutional Review Board. Additional details can be found in Stewart et al.{Stewart:2017ba}

B. Hydrogels. Polyethylene glycol (PEG) methyl ether acrylate and PEG diacrylate were combined in 95:5 w:w ratios. The total polymer of 25 wt% in water was vortexed, and Irgacure (2-hydroxy-4'-(2-hydroxyethoxy)-2-methilpropiophenone) was added and used as the photo-initiator. The samples were poured into petri dishes,exposed to UV to obtain 3 mm thick polymerized samples, and stored in DI water. Gelatin-alginate "Capgel" cubes were kindly donated by Dr. Bradley Willenberg from the University of Central Florida and stored in phosphate buffer saline (PBS).{DellaRocca:2012hx, DellaRocca:2016dv}

Supplemental Table 1. Mechanical characterization of similar materials to demonstrative materials

Material	Effective Modulus [kPa]	Comments	Steady-State Modulus [kPa]	Comments
Human Pancreas	~1 - 25	Tissue from patients undergoing pancreatic-duodenectomy; mesoscale indentation fit to Hertz model{Sugimoto:2014eh}	1-14	Normal, inflamed, and tumor tissue; mesoscale indentation fit to Hertz model and SLS{Rubiano:2017dx}
	0.56 – 2.49	*This work*	~2	*This work*
Rat Myocardium	18 ± 2	AFM indentation fit to Hertz model {Berry:2006hs}	15.0 ± 4.5	Flat-punch mesoscale indentation fit to Hertz model and SLS{Rubiano:2016ub}
	27.5 – 41.0	*This work (Indentation rate: 3.6-36 μm/s)*		
Poly-acrylamide 4.5%A:0.075 %Bis	~0.5 - 3	AFM indentation fit to Hertz model using 5% acrylamide (A) and similar bisacrylamide crosslinker (Bis) {Engler:2004hy, Tse:2001ft}	~5 - 10	Quasi-static mesoscale indentation fit to Hertz model for 5%A:0.025%Bis{Gautreau:2006tk}
	~2	*This work*		
0.4% Agarose	4.3 – 8.1	*This work (Indentation rate: 15-60 μm/s)*	~3	Converted from shear modulus calculated by computational model of quasi-static mesoscale indentation{Anonymous:2011bd}
0.6% Agarose	~3 - 10	Hertz-type models of flat-punch indentation for 0.75% agarose{DelaineSmith:2016co}	~0.5 - 2	Hertz-type models of flat-punch indentation for 0.75% agarose{DelaineSmith:2016co}
			~6	Converted from shear modulus calculated by computational model of quasi-static mesoscale indentation{Anonymous:2011bd}
	9.7 – 15.4	*This work (Indentation rate: 15-300 μm/s)*	~8	*This work*
CY52-276 Silicone	~30	*This work (Indentation rate: 3 μm/s)*	~5 - 9	Quasi-static mesoscale indentation{Bashirzadeh:2018fa}
Collagen (2 mg/mL)	< 1	Cell-embedded (1.6 mg/ml) collagen gels, AFM indentation fit to Hertz model{Anonymous:2014hs}	< 2.2	Predicted from tensile test at different strain rates{LopezGarcia:2010gk}
	~0.5	*This work (Indentation rate: 1 μm/s)*		
Porcine Kidney			~0.6	Stress relaxation using rheometer; intact (not decellularized) sample{Nasseri:2002fd}
	~1.5 – 3.5	*This work (decellularized)*	~1	*This work (decellularized)*

Supplemental Table 2. Example uncertainty on metrics used to calculate transient modulus from Equation 3 for our experimental setup. Sources and degree of error must be determined independently for each experimental setup.

Parameter	Dependencies/Sources of error	Estimation of Error
$F(t)$, Force	Cantilever stiffness: 2% on calibrated value Sensor precision: 0.2% Cantilever vibration: ±15 μN at 10 μm/s displacement rate while in contact	For low modulus materials, cantilever vibration dominates uncertainty , e.g. 15% for indentations up to ~100 μN. For higher modulus materials where indentation forces reach mN values, cantilever stiffness dominates error.
ν, Poisson's ratio	Hard to calculate in soft matter, estimates range from 0.3-0.5	Up to ±10% for typical ranges of force and depth
R, Radius of indenter tip	625 nm tolerances	Negligible, <0.05% for tips used in this work
$\delta(t)$, Indentation depth	Piezo Stage Linearity Error: 0.02% Piezo Stage Resolution: 0.5 nm Capacitive sensor resolution of deflection: 2.1 nm at 100 Hz acquisition	Negligible, <<0.05% for typical indentations

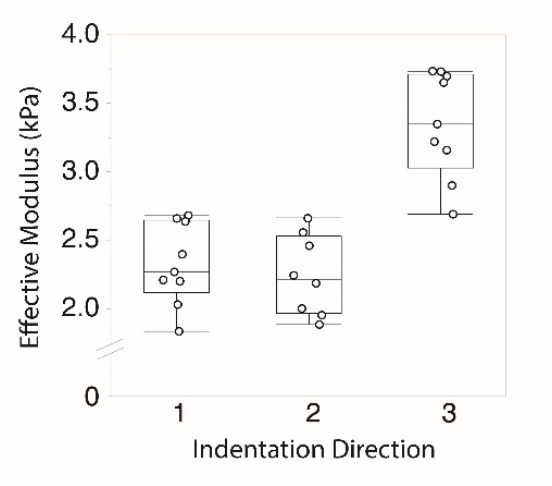

Supplementary Figure A. SSM for Capgel cube indented in three orthogonal orientations show that its anisotropy due to the direction of the fibers requires a more sophisticated model to obtain reliable results.

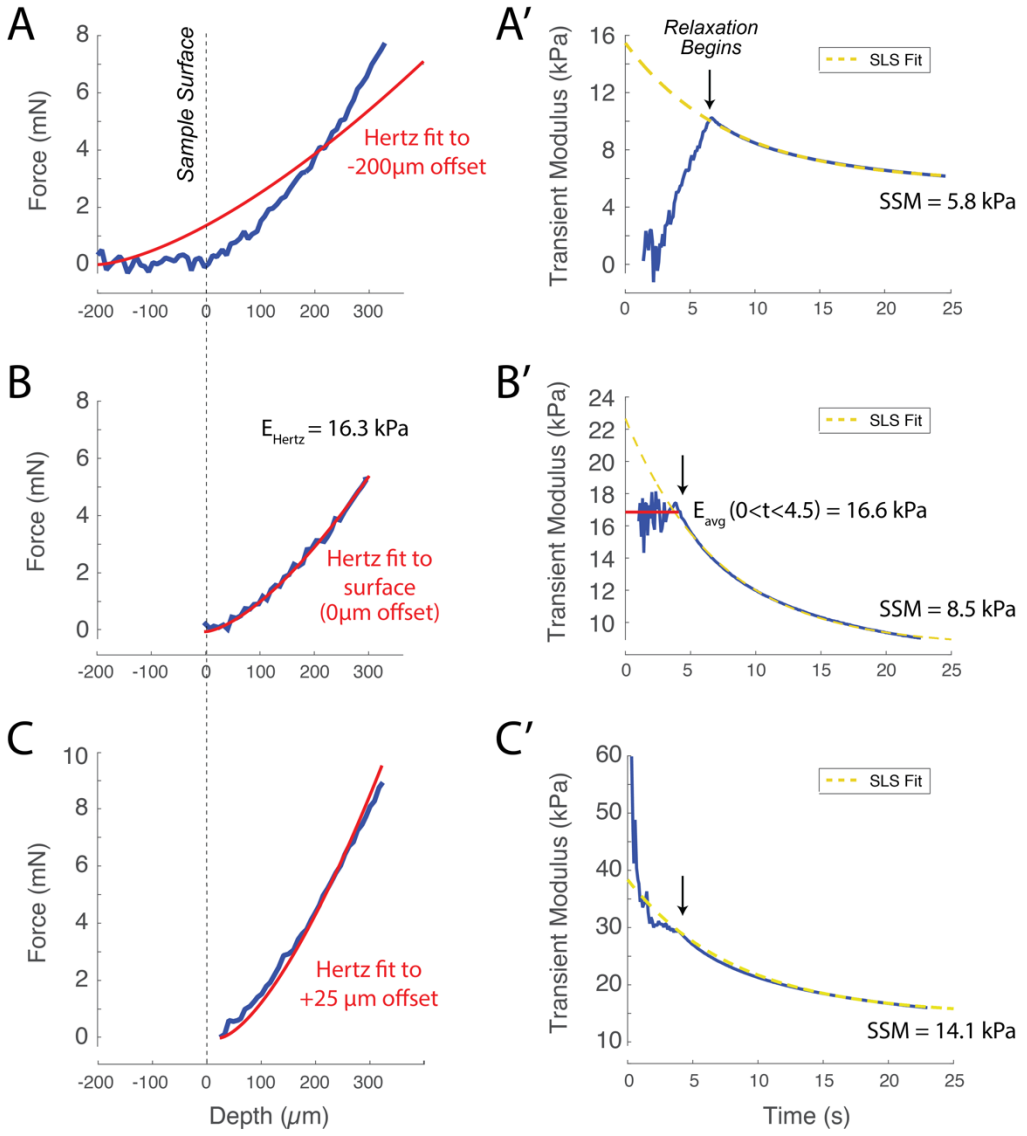

Supplementary Figure B. Accurate identification of sample surface is necessary for consistent Steady-State Modulus (SSM) results as demonstrated on 0.6% Agarose gels. (A-C) Force-displacement data of indentation phase with Hertzian fit and (A'-C') transient modulus for indentation and relaxation phases emphasize outcomes of poor surface-finding for samples indented (A,A') beginning 200 µm away from the surface, (B,B') beginning at the surface, and (C,C') beginning 25 µm into the sample. Vertical arrows indicate beginning of relaxation phase for respective panels. (A,A') Erroneously fitting to data acquired before making contact yields artificially low values for SSM. (B,B') The average of the transient modulus during the loading stage closely matches the effective modulus when the indentation acquisition begins accurately on the surface of the sample. (C,C') If the sample is pre-indented when the cycle begins, the effective modulus from a Hertzian fit and the SSM are artificially high. Yellow dashed lines represent the Standard Linear Solid (SLS) model fit for the relaxation curves (see section 3.4 for discussion).

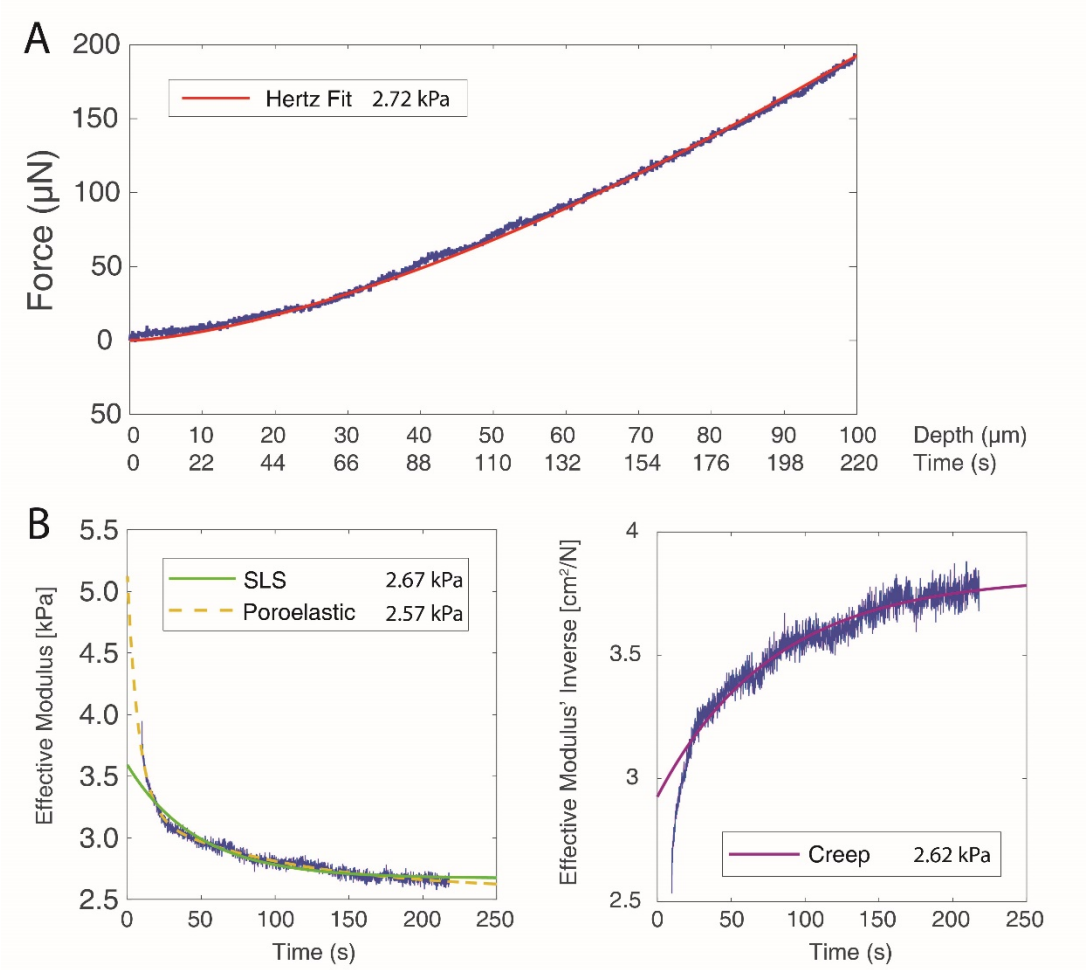

Supplementary Figure C. Quasi-static indentation of biological material yields similar effective modulus to Steady-State Modulus (SSM) from stress relaxation experiments. (A) Quasi-static indentation of hydrated 1 mm-thick human pancreatitis sample to 10% sample thickness is fit to a Hertz model and yields a reduced modulus of 2.72 kPa. (B) After allowing strain recovery for 5 minutes, the same spot was indented using a 10 second loading phase and a 210 second stress relaxation phase. Three time-dependent elasticity models (Supplementary Table 1) were used to obtain the SSM, reported inside the graph legend.

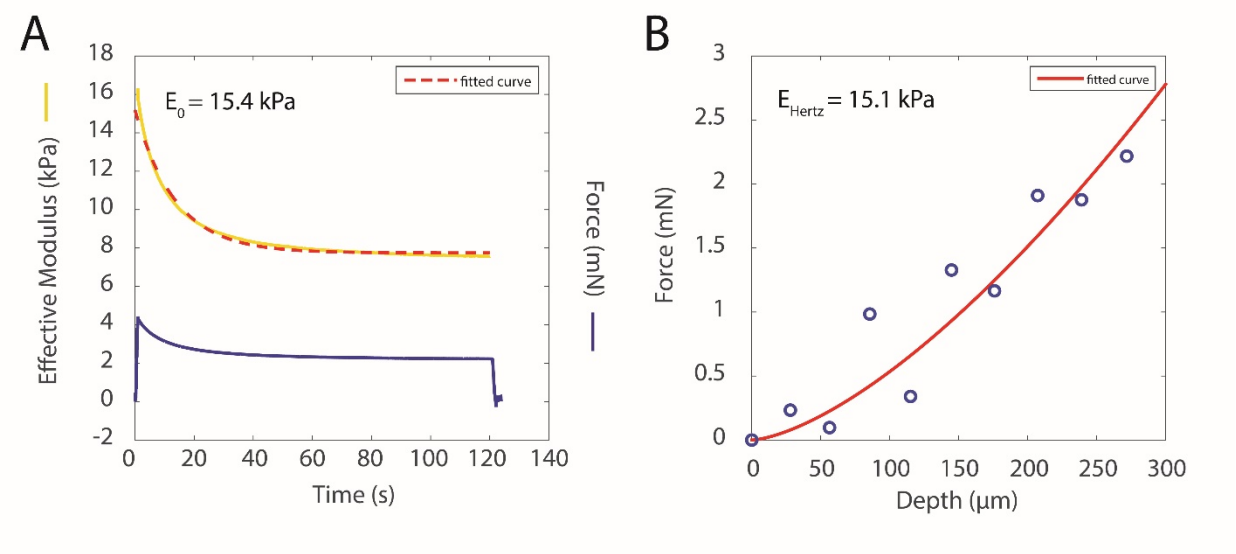

Supplementary Figure D. Quasi-instantaneous indentation of hydrogel enables calculation of initial modulus, E_0, from transient modulus equation (Equation 3) to yield approximately the same effective modulus (15.4 kPa) of a one-second loading curve at a modest acquisition frequency of 10 Hz (15.1 kPa, NMSE = 0.8716). (A) Force and elastic modulus as a function of time (same y-axis values, units as indicated) for a 120s relaxation indentation, showing an SLS fit in red dashed line. (B) Force-displacement data points during loading including Hertz fit (Equation 2) in red solid line. Indented sample: Agarose 0.6% hydrogel.

Supplementary Table 3. Constitutive Models to Calculate Steady-State Modulus from Transient Modulus Data: Standard Linear Solid Model, Two-Maxwell-Element Model, and Generalized Kelvin Model for Creep Experiments.

Model	Schematic	Governing Equation
Standard Linear Solid	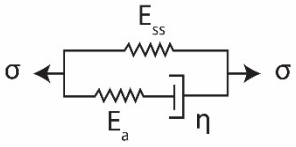	$E(t) = E_{ss} + E_a \cdot e^{-\frac{t}{\tau}}$ [4]
Two-Element Maxwell	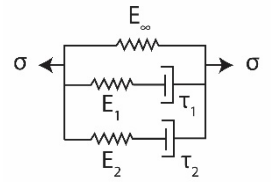	$E(t) = E_\infty + E_1 \exp\left(-\frac{t}{\tau_1}\right) + E_2 \exp\left(-\frac{t}{\tau_2}\right)$ [5]
Generalized Kelvin Model	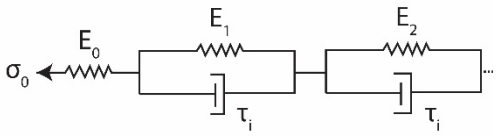	$\frac{\varepsilon(t)}{\sigma_0} = \frac{1}{E_0} + \sum_{i=1}^{n} \frac{1}{E_i^*}\left(1 - e^{-\frac{t}{\tau^*}}\right)$ [6]

Eqn. 4: E_{ss}: steady-state modulus. E_a: additional strain-rate dependent modulus. τ: time constant.
Eqn. 5: E_∞: steady-state modulus. E_i: strain-rate dependent elastic moduli. τ_i: time constants.
Eqn. 6: σ_0: constant applied stress. E_i: elastic moduli. ε: strain, time function. τ: time constants.

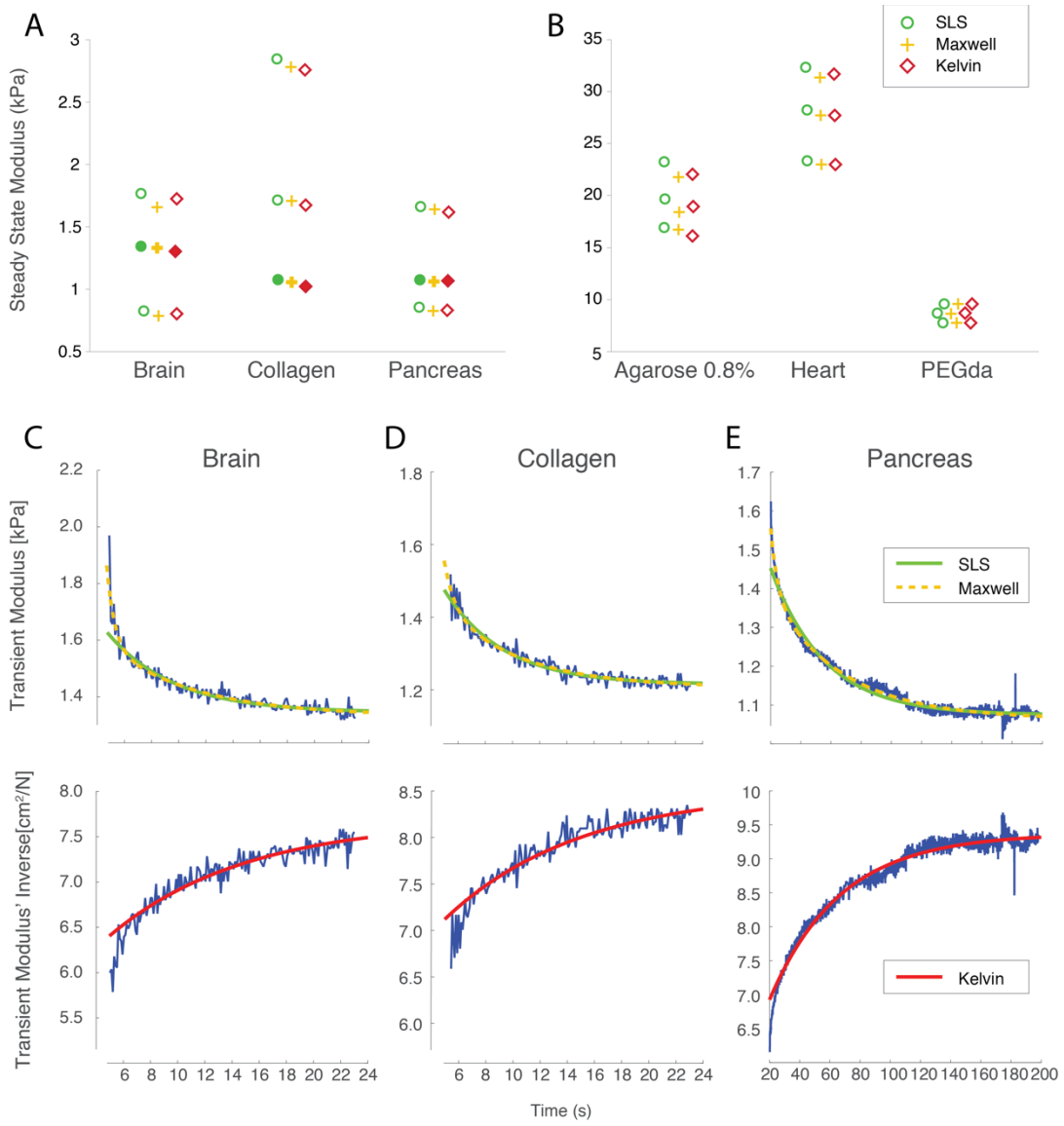

Supplementary Figure E. Steady-State Modulus is consistent when fitted using three different constitutive models. (A-B) Force-displacement curves were obtained from indentations on three complaint materials (A) and three relatively stiff materials (B). At least six indentation were performed on each sample (one sample per sample type), and representative low, medium, and high SSM data were selected from each of the 6 categories of materials tested. Force-displacement data was then used to obtain an equivalent SSM as fit to three distinct time-dependent constitutive models (see Supplementary Table 1). Each cluster of three markers represents one indentation and resulting equivalent SSMs calculated from the three constitutive models as referenced in legend. (C-E) Transient Modulus plots fit to three time-dependent models (see Table 1) for indentations on soft materials yielding SSM between 1 and 1.5 kPa. Fits demonstrate that even though the instantaneous modulus and initial relaxation behavior may vary depending on the selected model, the SSM is consistent. Data shown in (C-E) are indicated in (A) with solid markers.